JOURNAL OF CHEMICAL INFORMATION AND MODELING

Article

pubs.acs.org/jcim

Concerted Movement in pH-Dependent Gating of FocA from Molecular Dynamics Simulations

Zhiwei Feng, Tingjun Hou, and Youyong Li*

Institute of Functional Nano & Soft Materials (FUNSOM) and Jiangsu Key Laboratory for Carbon-Based Functional Materials & Devices, Soochow University, Suzhou, Jiangsu 215123, China

Supporting Information

ABSTRACT: FocA, a member of the formate-nitrite transporter (FNT) family, transports formate and nitrite across biological membranes in cellular organisms. The export and uptake of formate in bacteria are both mediated by FocA, which undergoes a pH-dependent functional switch. Recently, the crystal structures of *Escherichia coli* FocA (EcFocA), *Vibrio cholerae* FocA (VcFocA), and *Salmonella typhimurium* FocA (StFocA) were reported. We performed molecular dynamics (MD) on StFocA and EcFocA with different states of His209 (protonated and unprotonated), representing different pH conditions of FocA. The N-terminal helix in each protomer of StFocA covers and blocks the formate channel. At neutral or high pH (MD simulations with unprotonated His209), the concerted movement of the N-terminal helices of pairs of protomers of StFocA opens its formate channel. At low pH (MD simulations with protonated His209), protonated His209 interacts tightly with its neighboring residue Asn262, and the channel becomes narrower, so that the formate can hardly pass through the channel. We obtained similar results for EcFocA. Our study shows that pairs of protomers of FocA move in a concerted way to achieve its pH-dependent gating function, which provides information on the dynamics of the gating mechanism of FNT proteins and aquaporins.

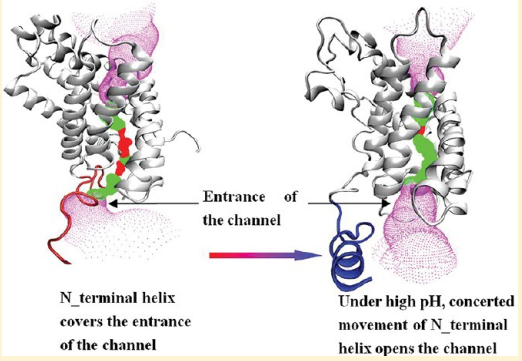

1. INTRODUCTION

Transport of small solutes across biological membranes is fundamental for cellular organisms. Aquaporins[1−8] are a superfamily of integral membrane proteins that allow the rapid and highly selective flux of water and other small solutes across membranes.[9] Mutagenic, topological, and crystallographic analyses of aquaporins have revealed that the functional channels consist of a single polypeptide containing a water pore that is assembled in the membrane as tetramers.[9−12]

Formate is the major metabolite of enterobacterial mixed-acid fermentations in anaerobic environments.[13−15] Intracellular accumulation of formate can lead to a substantial decrease in cytoplasmic pH. Export of anionic formate across the cytoplasmic membrane is mediated by the formate channel FocA.

FocA is a typical member of the formate-nitrite transporter (FNT) family (transporter classification 2.A.44)[16] and serves as a channel for structurally similar short-chain acids such as formate and nitrite, in bacteria, archaea, fungi, algae, and parasites. The function and structure of FocA are reminiscent of those of other known members of the FNT family, including NirC, as characterized in *Escherichia coli* for nitrite uptake and export,[17−22] and FdhC, as described in *Methanobacterium thermoformicium* for the formate uptake.[16,23,24] These members of the FNT family share considerable sequence homology and have less sequence similarity with other proteins. Despite sharing less sequence homology with aquaporin, the structure and mechanism of FocA closely resemble those of aquaporin, the integral membrane protein that forms channels in the membrane.[25]

If the generation of a proton motive force through the respiratory oxidation of formate is no longer desirable or if the pH of the growth medium drops below 6.8, the bacteria switch to rapid reuptake of formate for dispropotionation into CO_2 and H_2.[26] The uptake of formate is also mediated by FocA, so that the protein must undergo a pH-dependent functional switch.[27]

Recently, crystal structures of FocA have been reported, including those of *Escherichia coli* FocA (EcFocA),[28] *Vibrio cholerae* FocA (VcFocA),[29] and *Salmonella typhimurium* FocA (StFocA).[30] In all three crystal structures, FocA is a symmetric pentamer consisting of five protomers (where a protomer is a structural unit of an oligomeric protein, as shown in Figure 1), and each protomer consists of six transmembrane helices. Moreover, the C-terminus and N-terminus of FocA are both placed on the cytoplasmic side, which is in agreement with the predicted topology of FocA.[27] Importantly, FocA has a center pore in its pentameric assembly and an axial pore in each of its protomers: the center pore seems to be occupied by lipid molecules within the plasma membrane of *E. coli*,[10,11,31,32] and the axial passage relates to the transport function.[28,29] In EcFocA,[28] potentially important channel residues were

Received: April 12, 2012
Published: July 2, 2012

   dx.doi.org/10.1021/ci300250q | *J. Chem. Inf. Model.* 2012, 52, 2119−2131

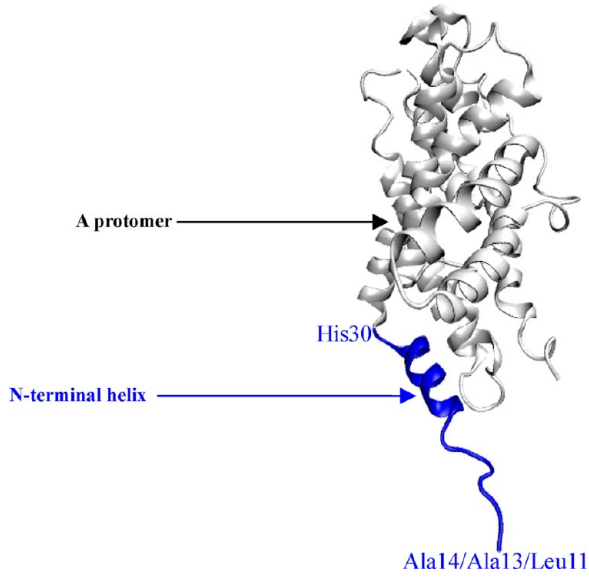

Figure 1. Cartoon showing a N-terminal helix in a protomer. The N-terminal helix consists of 17/18/20 residues (from Ala14/Ala13/Leu11 to His30) in the crystal structure, as highlighted in blue color. A protomer is a structural unit of an oligomeric protein. FocAs have five protomers.

identified, the channel path was defined, and two constriction sites were revealed. In VcFocA,[29] two different conformations of a Ω loop region in the structure were described, suggesting that the Ω loop plays a critical role in the gating of VcFocA. In StFocA,[30] three states were observed in the protomers of the pentameric channel in the presence of the N-terminal helix region [from residue 11/13/14 (Lue11/Ala13/Ala14) to residue 30 (His30), as shown in Figure 1], suggesting a possible mechanism of FocA gating.

All three crystal structures[28−30] revealed that the highly conserved residue His209 (His208 in VcFocA) is located vertically on the periplasmic side of the slot and lines on the side of the pore cavity, with its imidazole side chain pointing toward the cytoplasmic side. This residue directly interacts with the important residues along the axial passage, suggesting that its side-chain rotamer might play a key role in the activation mechanism. The other five histidine residues (and other aspartate and glutamate residues) in each protomer are not located along the entrance, so they hardly affect the conformation of the entrance and are harder to protonate than His209. (Detailed analysis can be found in section 2.)

To study the pH-dependent gating of the FocA channel, we performed molecular dynamics (MD) simulations on StFocA and EcFocA (the sequence identity and sequence similarity between EcFocA and StFocA are 85.2% and 88.2%, respectively) with different states of His209 (protonated and unprotonated) to represent different pH conditions of FocA (low pH and neutral/high pH, respectively). The MD simulations were performed in explicit water and lipid for 20 ns. We found that, at neutral/high pH (MD simulations with unprotonated His209), the concerted movement of the N-terminal helices of pairs of protomers of StFocA opens its formate channel. At low pH (MD simulations with protonated His209), protonated His209 interacts tightly with its neighboring residue Asn262, and the channel becomes narrower, making formate hardly able to pass through the channel. We obtained similar results for EcFocA. Our study shows that the pairs of protomers in FocA move in a concerted way to achieve its pH-dependent gating function, which is consistent with studies of aquaporins[33−37] and provides information on the dynamics of the gating mechanism.

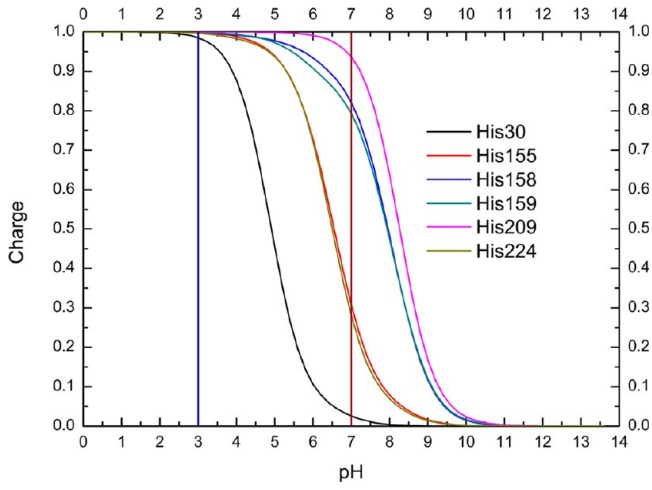

Figure 3. Comparison of the relationships between charge and pH for histidines, showing that His209 is easier to protonate than the other five histidines.

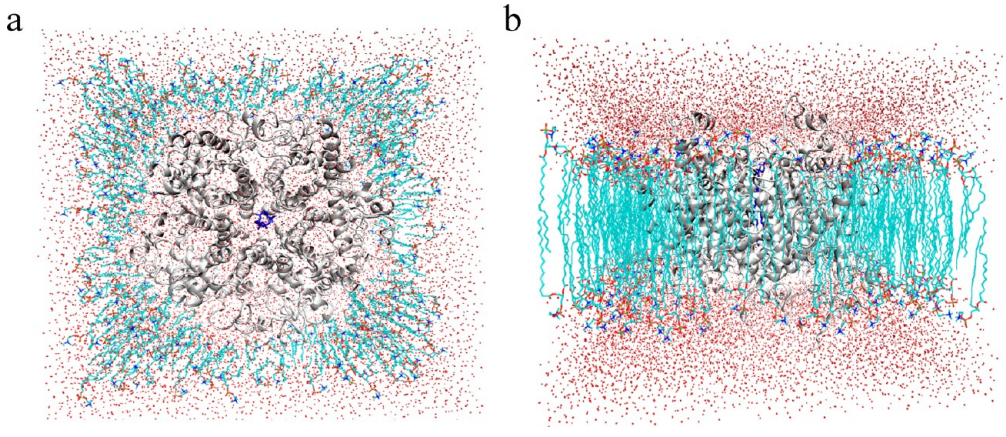

Figure 2. Molecular dynamics simulation box of StFocA/EcFocA with lipid and water: (a) top view from the periplasmic side, (b) side view from the membrane side. The box size was 120 × 120 × 90 Å^3, and 92641 and 101312 atoms were included in the periodic cell for StFocA and EcFocA, respectively. To solvate FocA's central lipid-filled cavity (central pore), one POPC molecule (blue licorice) was placed inside.

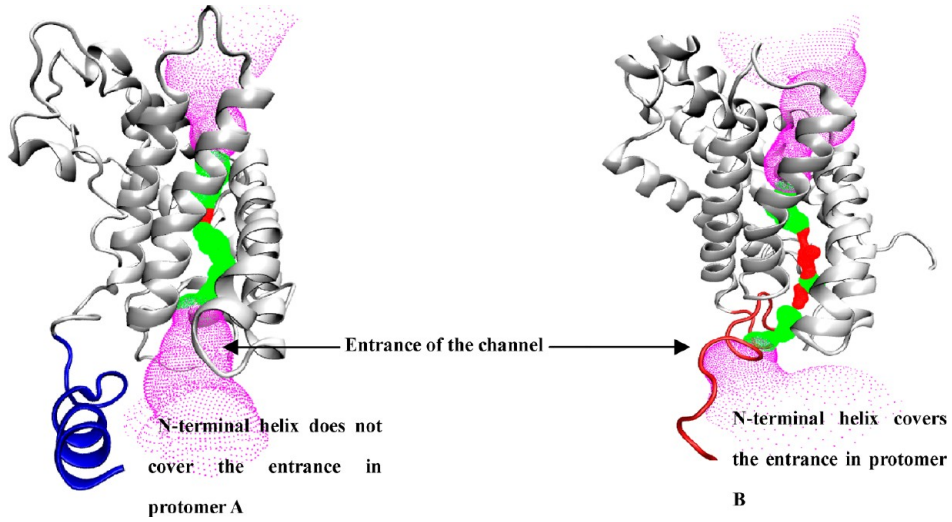

Figure 4. Transport channels of protomers A and B in the StFocA crystal structure. The entrance of protomer B is covered by its N-terminal helix and is in the closed state. In comparison, the entrance of protomer A is only slightly covered by its N-terminal helix and is in the intermediate state.

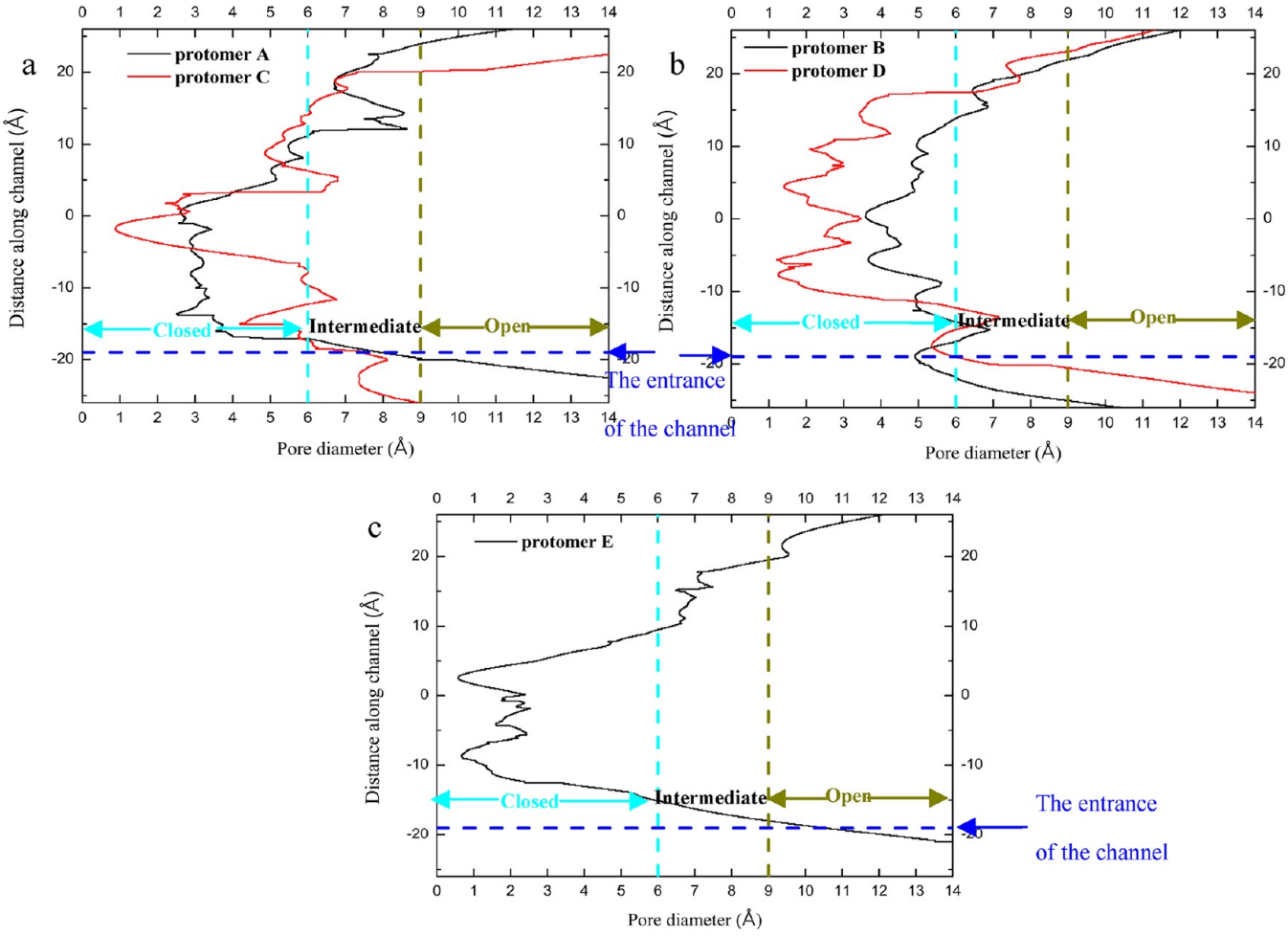

Figure 5. Diameter of the transport channel of each protomer of StFocA as a function of the distance along the channel. The horizontal dashed line represents the position of Cα of residue Pro31 along the transport channel, and the diameter of the transport channel at that position is defined as the diameter of the entrance of the transport channel. For the crystal structure of StFocA, protomers A (7.8 Å) and C (7.4 Å) are in the intermediate state. Protomers B (4.9 Å) and D (5.8 Å) are in the closed state. Protomer E (10.2 Å) is in the open state.

dx.doi.org/10.1021/ci300250q | J. Chem. Inf. Model. 2012, 52, 2119−2131

2. MATERIALS AND METHODS

2.1. Protein Structures. The crystal structures of FocA *Salmonella typhimurium* (StFocA)[30] (PDB entry 3Q7K, resolution 2.8 Å) and FocA *Escherichia coli* (EcFocA)[28] (PDB entry 3KCV, resolution 3.2 Å) were used in our studies. These structures were retrieved from the Protein Data Bank (http://www.pdb.org/pdb/).

To solvate FocA's central lipid-filled cavity (central pore), one 1-palmitolyl-2-oleoyl-*sn*-glycero-3-phosphocholine (POPC) molecule was placed manually by selecting from a superimposed pre-equilibrated POPC bilayer lipid molecules that did not clash with the surrounding protein (Figure S1 in the Supporting Information).

2.2. MD Simulations. The crystal structures were prepared using Discovery Studio[38] (including residue repair and energy minimization). The missing loops near the cytoplasmic surface of protomers B, D, and E were built using Discovery Studio.[38] The N-terminal helix of protomer E was not resolved in the crystal structure. The N-terminal helix is long and cannot be built accurately by modeling, so we did not include the N-terminal helix of protomer E in our simulations.

The protein was embedded in a pre-equilibrated (120 × 120 Å^2) and periodic structure of POPC. The lipid molecules

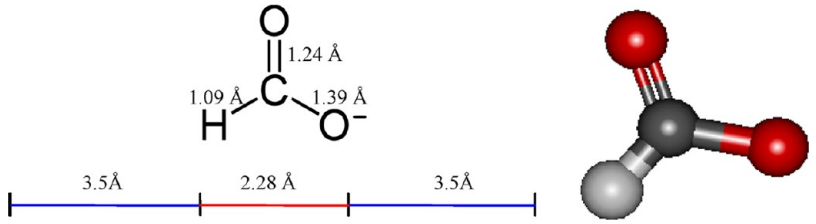

Figure 6. Chemical structure of formate. The diameter of formate is about 2.28 Å.

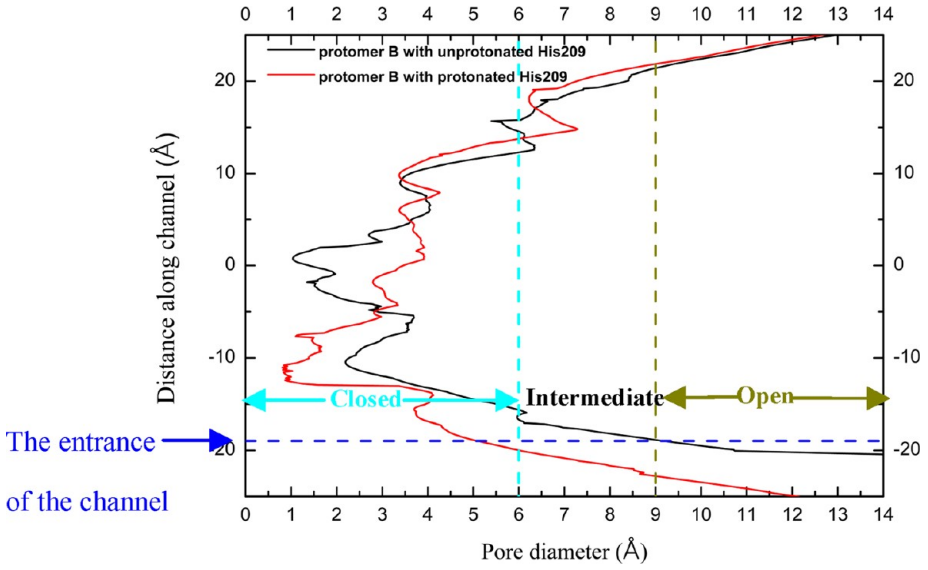

Figure 7. Diameter of the transport channel of protomer B of StFocA as a function of the distance along the channel after 20-ns MD simulations with unprotonated His209 (neutral/high pH) and with protonated His209 (low pH). At neutral/high pH, protomer B changes its state from closed to open. At low pH, protomer B maintains its closed state.

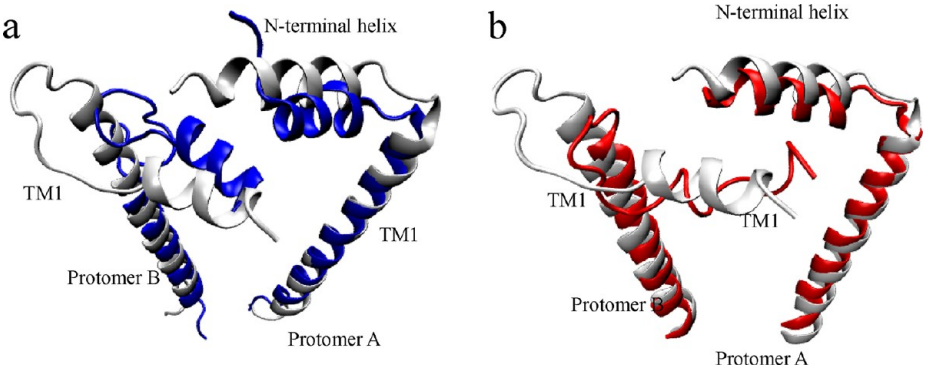

Figure 8. Representation of the concerted movement of the N-terminal helices of protomers A and B, which eventually opens the transport channel of protomer B at neutral/high pH. Crystal structure of StFocA at pH 4.0 (gray) and structures of StFocA equilibrated by MD at (a) neutral/high pH (blue) and (b) low pH (red).

dx.doi.org/10.1021/ci300250q | J. Chem. Inf. Model. 2012, 52, 2119−2131

within 5 Å of the complex were eliminated. Then, we inserted the resulting structure into a water box [three-site transferable intermolecular potential (TIP3P) water model[39]] and eliminated the water molecules within 5 Å of the lipid and protein. The MD simulation system was constucted using VMD.[40]

The overall system (Figure 2) contained the protein, 226 lipid molecules, ~17269 water molecules, and 5 sodium ions for a total of ~101312 atoms per periodic cell. The box size was 120 × 120 × 90 Å^3. The system was first equilibrated for 500 ps with the protein fixed. Then, the protein was released, and another 500-ps equilibration was performed.

Starting from the last frame of the equilibration, we performed 20-ns MD simulations. The MD simulations were performed using the NAMD[41] package (version 2.7b2) with the CHARMM27[42−44] force field for the studied complex with explicit water and periodically infinite lipid. Electrostatics were calculated using the particle mesh Ewald (PME)[45] method with a 12-Å nonbonded cutoff and a grid spacing of 1 Å per grid point in each dimension. The van der Waals energies were calculated using a smooth cutoff (switching radius = 10 Å, cutoff radius = 12 Å). The temperature and pressure were kept constant using a Langevin thermostat and a Langevin barostat, respectively. The time step of the MD simulations was set to 1 fs. Data were saved every 10 ps for analysis. MD simulations of 20-ns duration were performed at a constant temperature of 310 K and a constant pressure of 1 atm. Trajectory analyses were carried out with VMD.[40,46−49]

Histidine residues ionize within the physiological pH range (~7.4). To mimic the effects of pH, the protonation states of the His residue were considered generally. In our simulations, protonated His was used to represent neutral/high-pH conditions, whereas unprotonated His represented low-pH conditions. Specifically, we considered that protonation occurred for pH < pK. To determine the protonation states for histidines, we used Discovery Studio 2.5[38] to predict protein ionization and residue pK values. The pK values calculated for the histidines were as follows: His30, 4.91; His155, 6.56; His158, 7.96; His159, 7.94; His209, 8.26; and His224, 6.50. Figure 3 shows the relationships between the charge and pH of histidines in protomer D (calculated with Discovery Studio 2.5). The other four protomers of FocA show the similar results. Figure 3 shows that His209 is easier to protonate than the other five histidines between pH 3 and pH 7 in FocA. Moreover, the calculated pK values of the aspartate (Asp88, 4.65; Asp154, 3.88; Asp190, 3.32; Asp225, 5.30; Asp253, 3.86) and glutamate (Glu20, 4.73; Glu21, 4.39; Glu137, 5.75; Glu163, 3.74; Glu208, 5.19; Glu230, 4.30; Glu240, 4.27) residues were found to be smaller than that of His209. Aspartate and glutamate are harder to protonate than histidine. The pK values of the residues (His30, 4.91; Glu20, 4.73; Glu21, 4.39) in the N-terminal helix were all found to be smaller than that of His209. In addition, His209 is located at a critical position in the channel and has been reported to be important for FocA's function. Thus, we compare MD results for different protonation states of His209.

We performed MD simulation of FocA with protonated His209 and unprotonated His209 to represent different pH conditions and describe the effects of pH on the structure/function of FocA.

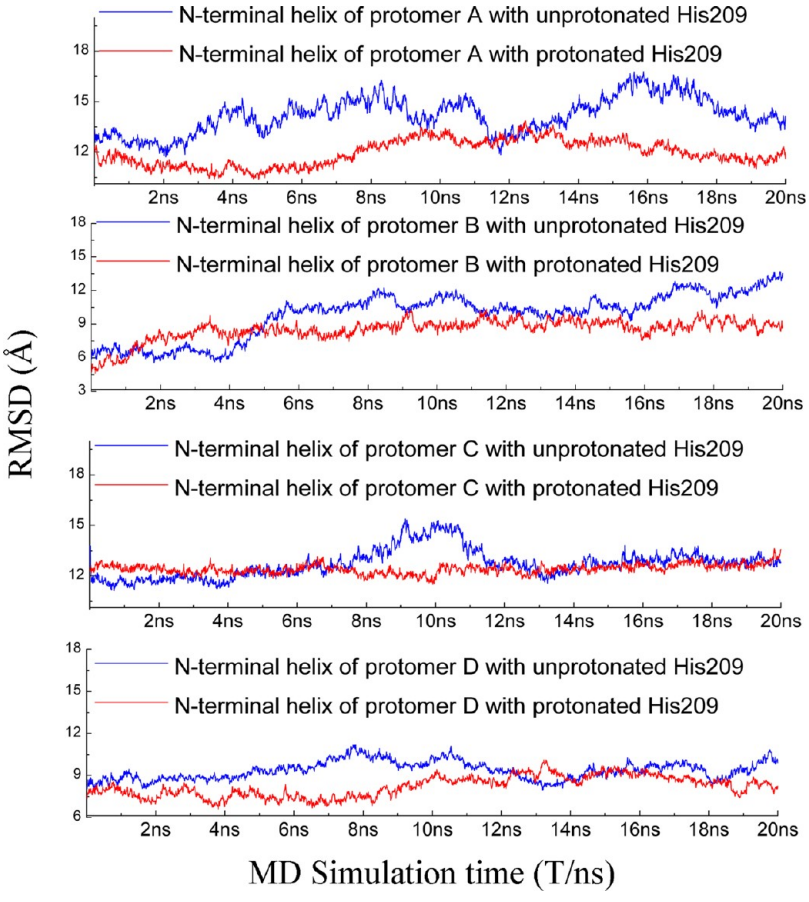

Figure 9. Time evolutions of the rmsd values of the N-terminal helices of four protomers at neutral/high pH (with unprotonated His209, blue) and low pH (with protonated His209, red).

In this work, we use the phrase "with protonated His209" to represent MD simulations at low pH and the phrase "with unprotonated His209" to represent MD simulations at neutral/high pH.

3. RESULTS AND DISCUSSION

3.1. Formate Channel and Open/Closed States of the Protomers of FocA. The overall structure of each StFocA, EcFocA, and VcFocA is formed by five protomers with the termini of the peptide chain on the cytoplasmic side of the membrane, as shown in Figure 2. In each protomer of FocA, a continuous channel crosses the membrane, creating a pore with funnel-like openings on both sides of the membrane. Figure 4 shows the transport channel of two protomers (protomers A and B) of StFocA, which was visualized using HOLE.[24,50] Figure 5 shows the diameters of the transport channels of the five protomers of the StFocA crystal structure as functions of the distance along the channel. The narrowest part of each channel is in the middle of the transport channel, which is flexible to accommodate the passage of formate and other small molecules.

The entrance of the transport channel is controlled by the conformation of the N-terminal helix, as shown in Figure 4, which plays a critical role in opening and closing the transport channel. To define the diameter of the entrance of the transport channel, we selected Cα of residue Pro31 in each protomer as the reference point, because Pro31 is the last residue of the N-terminal helix and the first residue of TM1 (transmembrane domain 1).

The diameter of formate is 2.28 Å, as shown in Figure 6. To accommodate formate in the entrance of the transport channel, the diameter of the entrance needs to be 9 Å for formate to have favorable van der Waals interaction distances on both sides, that is, 3.5 Å on each side (see Figure 6). We define the transport channel as being in the "open state" when the diameter of its entrance is greater than 9 Å. When the diameter of the entrance of the transport channel is less than 6 Å, it is not plausible for formate to enter the channel, so we define the transport channel as being in the "closed state" when the diameter of its entrance is less than 6 Å. When the diameter is between 6 and 9 Å, we refer to the transport channel as being in the "intermediate state". In Figure 5, diameters of 6 and 9 Å are highlighted in cyan and brown dashed lines, respectively.

In the crystal structure of StFocA, the diameters of the entrances of protomers A and C are 7.8 and 7.4 Å, respectively (Figure 5a), so these protomers are in the intermediate state. Protomers B (4.9 Å) and D (5.8 Å) are in the closed state (Figure 5b), whereas protomer E (10.2 Å) is in the open state (Figure 5c).

3.2. MD Simulations of FocA at Neutral/High pH and Low pH. After minimization of the structure of StFocA, we performed MD simulations of StFocA in explicit water and lipid with unprotonated His209 and protonated His209, representing neutral/high pH and low pH, respectively. We compared these two MD trajectories systematically to identify the differences in StFocA under different pH conditions.

During 20-ns MD simulations, the total energy of the system equilibrated within 4 ns, as shown in Figure S2 (Supporting Information). Thus, 20 ns is a reasonable time scale for our purposes of comparing the differences in FocA under different pH conditions.

As shown in Figure 7, at neutral/high pH, the diameter of the entrance expanded toward to 9.1 Å, and protomer B changed its state from closed to open. At low pH, the diameter of the entrance remained less than 6 Å, and protomer B maintained its closed state. Our MD results thus show that protomer B gates in a pH-dependent manner.

The other four protomers maintained their original states during our MD simulation. Specifically, protomers A and C were in the intermediate state, protomer D was in the closed state, and protomer E was in the open state. More details can be found in the Supporting Information (Figure S3). By analyzing the MD trajectories, we found that the N-terminal helices of pairs of protomers (A/B, C/D) move in a concerted way. For example, the N-terminal helix of protomer A moves in a concerted way with the N-terminal helix of protomer B, which eventually opens the transport channel of protomer B. (See the next section for details.)

3.3. Concerted Movement in FocA's pH Gating Function. In Figure 8, we show the structure of StFocA after an MD simulation aligned with the original crystal structure to highlight the difference.

As shown in Figure 8a, during 20-ns MD simulations with unprotonated His209, the N-terminal helices of protomers A

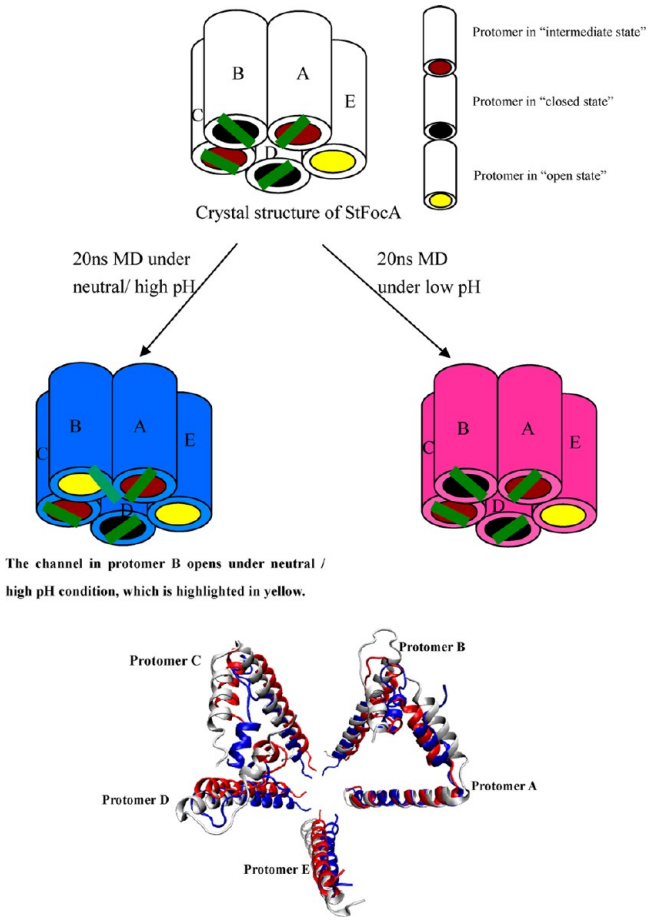

Figure 10. Results of 20-ns MD simulations performed for StFocA with unprotonated His209 (neutral/high pH) and protonated His209 (low pH). The N-terminal helix of each protomer could cover and block the formate channel. Each protomer of StFocA has three different conformations based on the coverage of the formate channel by the N-terminal helix: open (O), intermediate (I), and closed (C). At neutral/high pH, the concerted movement of protomers A and B opens the formate channel of protomer B (C → O) within 20 ns (highlighted in yellow). The N-terminal helix of each protomer moves in concert with its neighbor (blue for neutral/high pH, red for low pH).

dx.doi.org/10.1021/ci300250q | J. Chem. Inf. Model. 2012, 52, 2119−2131

and B were found to move in a concerted way, eventually causing the transport channel of protomer B to open. Meanwhile, the KTFYLAI motif of TM1 (residues 33−39) in protomer B broke into a coil, which facilitated the opening of the channel of protomer B.

In contrast, with protonated His209, the N-terminal helices of protomers A and B did not move significantly (Figure 8b), and the channel of protomer B remained in the closed state at low pH.

The N-terminal helix of protomer C was found to prohibit the movement of the N-terminal helix of protomer D in both MD simulations. Protomers C and D maintained their states, namely, the intermediate state and the closed state, respectively. (More information can be found in Figure S4 of the Supporting Information.) For protomer E, there is no N-terminal helix to cover the transport channel in the crystal structure. Protomer E was thus found to remain in the open state.

Figure 9 shows the time evolutions of the rmsd values of the N-terminal helices. The rmsd values of the N-terminal helices at neutral/high pH (blue line) are large, indicating that the N-terminal helices make significant movements. At neutral/high pH, the N-terminal helices of protomers A and B make significant movements, opening up the transport channel of protomer B.

Figure 10 summarizes the influence of protonated or unprotonated His209 on each protomer of StFocA based on our MD results. At neutral/high pH (with unprotonated His209), the concerted movement of the A/B pair of

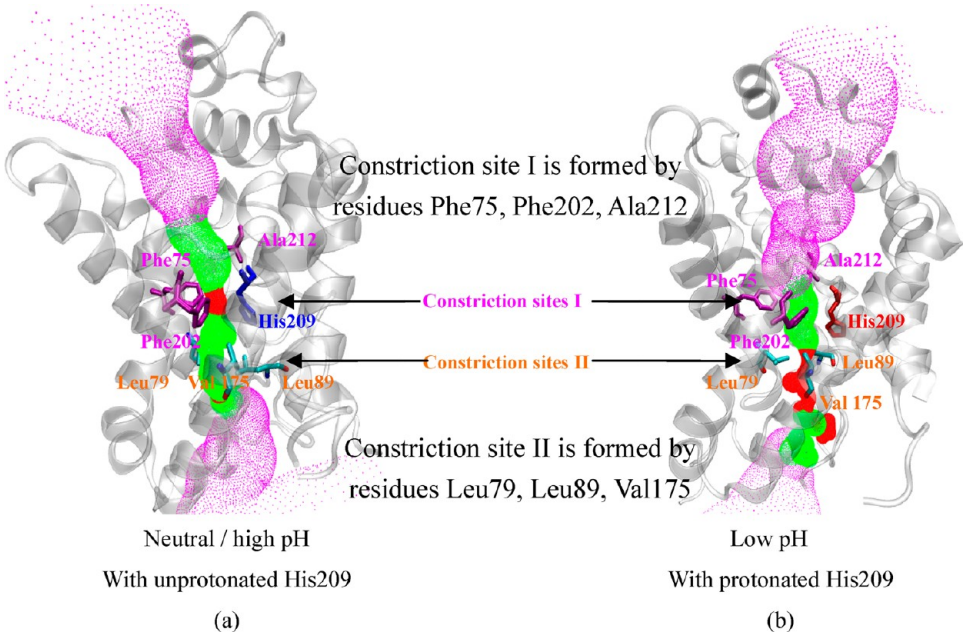

Figure 11. Formate channel of protomer B after MD simulations at (a) neutral/high pH and (b) low pH.

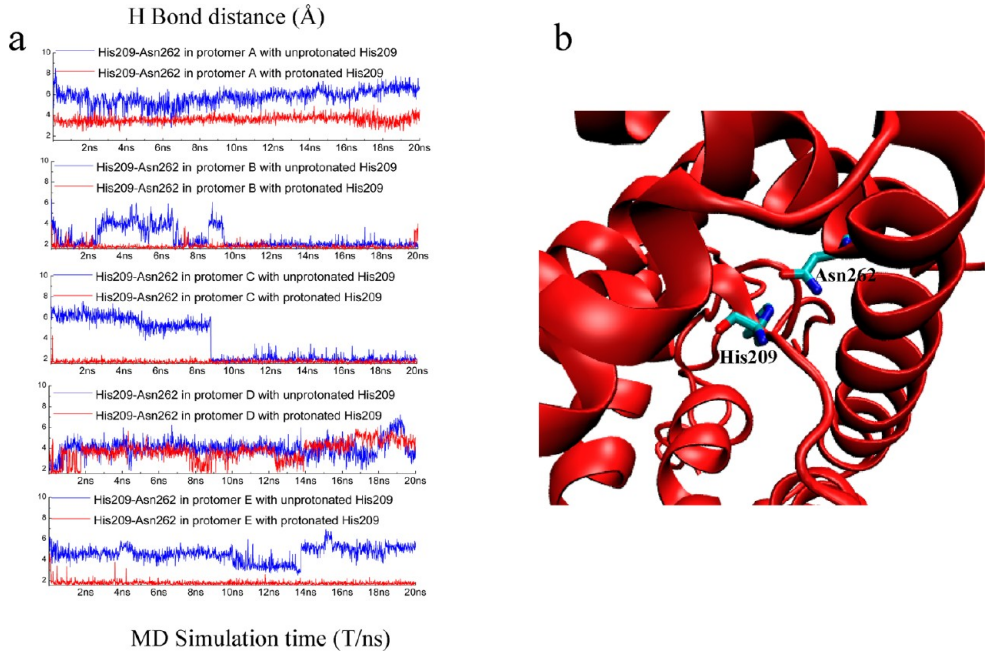

Figure 12. (a) Time evolutions of the hydrogen-bond distances between His209 and Asn262 in the five protomers of StFocA with protonated His209 (red line) and unprotonated His209 (blue line). (b) H-bond interaction between His209 and Asn262.

dx.doi.org/10.1021/ci300250q | J. Chem. Inf. Model. 2012, 52, 2119−2131

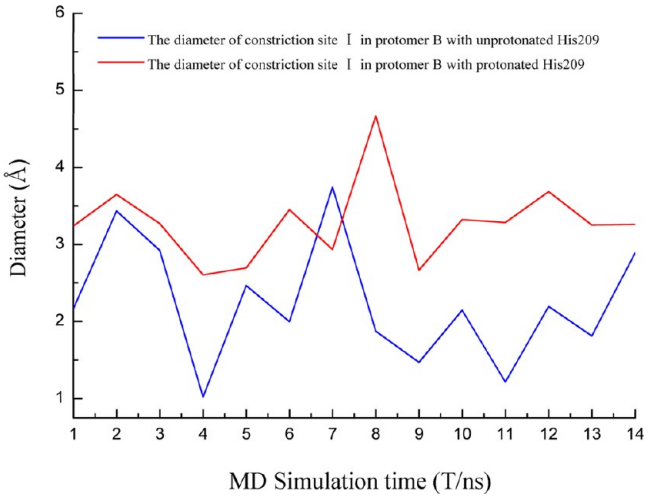

Figure 13. Time evolutions of the diameter of constriction site I in protomer B with unprotonated His209 (neutral/high pH, blue line) and protonated His209 (low pH, red line). The diameter of constriction site I was always larger with protonated His209 than with unprotonated His209.

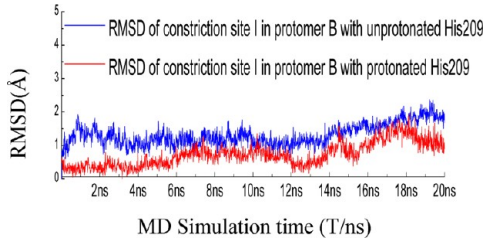

Figure 14. Time evolutions of the rmsd values of constriction site I in protomer B of StFocA, showing that constriction site I becomes less flexible with protonated His209.

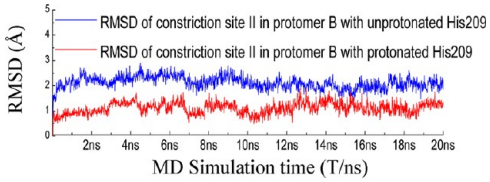

Figure 15. Time evolutions of the rmsd values of constriction site II in protomer B of StFocA showing that constriction site II also becomes less flexible with protonated His209.

protomers opens the formate channel of protomer B within 20 ns, as highlighted in yellow. Protomers A, C, D, and E maintain their original states: intermediate, intermediate, closed, and open, respectively. The rmsd values of protomers A–E are 3.6, 5.1, 5.3, 3.8, and 2.9 Å, respectively, at neutral/high pH. At low pH (with protonated His209), the five protomers keep the same states as in the crystal structure of StFocA. The rmsd values of protomers A–E in this case are 2.6, 4.3, 2.8, 3.0, and 2.2 Å, respectively. The protomers are more flexible at neutral/high pH than they are at low pH.

In summary, our simulation results showed that two pairs of protomers (A/B, C/D) move in concert. We did not include the N-terminal helix of protomer E in our simulations, because it is not resolved in the crystal structure. The function of N-terminal helix of protomer E remains unclear. It might or might not participate in the concerted movement of protomer pairs A/B and C/D. It should be flexible given that it is not resolved in the crystal structure. We assume that its high flexibility will facilitate the concerted movement of protomer pairs A/B and C/D.

During our MD simulations, we assigned all five protomers the same protonation states to make comparisons. We observed concerted movements of the N-terminal helices, which is important for FocA's function. The protonation process (picosecond time scale) occurs much more rapidly than the movement of the N-terminal helices (nanosecond time scale). Thus, it is justifiable for us to assign the same protonation[51,52] states of all five protomers and perform MD simulations to compare the movements of the N-terminal helices.

Our results are consistent with those of molecular dynamics simulations of aquaporins,[33−37] which indicated that aquaporins work asynchronously: At different pressures, the number of water molecules passing through each protomer is different.[37] For different protomers, the permeation events, signal-channel osmotic pressures, diffusive permeabilities, dihedral angles of important residues, distances between critical residues, and pore radii are also different.[33,35−37] Our results for FocA also indicate that protomers work not in a synchronous way, but in a concerted way.

3.4. Influence of Protonated or Unprotonated His209 on the Shape of the Channel. Figure 11 shows the formate channel of protomer B after MD simulations at neutral/high pH (Figure 11a) and at low pH (Figure 11b) as visualized with HOLE software. Constriction sites I and II are two narrow parts along the formate channel. Constriction site I is formed by Phe75, Phe202, and Ala212, whereas constriction site II consists of Leu79, Leu89, and Val175. Protonated His209 interacts tightly with its neighboring residue Asn262, making constriction site I larger. However, both constriction sites I and II become more rigid, making the formate hardly able to pass through the channel. (See the following analysis for details.)

(1). His209 Forms a H-bond with Asn262. There are several residues around His209, including Asn172, Thr91, and Asn262. We found that Asn262 interacts with His209 tightly when His209 is protonated. Figure 12a shows the time evolutions of the hydrogen-bond distances between His209 and Asn262 in the five protomers of StFocA. Figure 12b shows the locations of these two residues in the protomer. The hydrogen bond between His209 and Asn262 is more stable when His209 is protonated than when it is unprotonated. When His209 is protonated, it remains located vertically on the periplasmic side of the slot, lines on the side of the channel, changes the shape of the channel, and makes the channel less flexible. (See the following sections.)

(2). Constriction Site I Expands with Protonated His209 but Becomes Less Flexible at Low pH. To investigate the change in each axial channel caused by the protonation state of His209, we calculated the diameter of the pore in each protomer for 14 frames using HOLE;[24,50] the results are summarized in Tables S1 and S2 (Supporting Information).

The results in Table S1 (Supporting Information) show that the narrowest part of the axial channel appears in either constriction site I or constriction site II during 20-ns MD simulations with unprotonated His209 (neutral/high pH).

Comparison of the time evolution of the diameter of constriction site I in protomer B (Figure 13) shows that protonated His209 expands the diameter of constriction site I. Data for the other protomers led to similar conclusions. (See Tables S1 and S2 in the Supporting Information for details.)

However, constriction site I formed by Phe75, Phe202, and Ala212 became less flexible with protonated His209. Figures 14 and S5 (Supporting Information) show the results for protomer B and the other protomers.

With protonated His209, constriction site I became larger but also less flexible. This allows FocA to be a secondary active formate/H^+ importer at low pH.[30]

(3). Constriction Site II Also Becomes Less Flexible with Protonated His209. The results in Table S2 (Supporting Information) show that the narrowest part is constriction site II in each protomer with protonated His209 (low pH).

Meanwhile, constriction site II consisting of Leu79, Leu89, and Val175 also became less flexible because of the protonation of His209, making the formate hardly able to pass through the

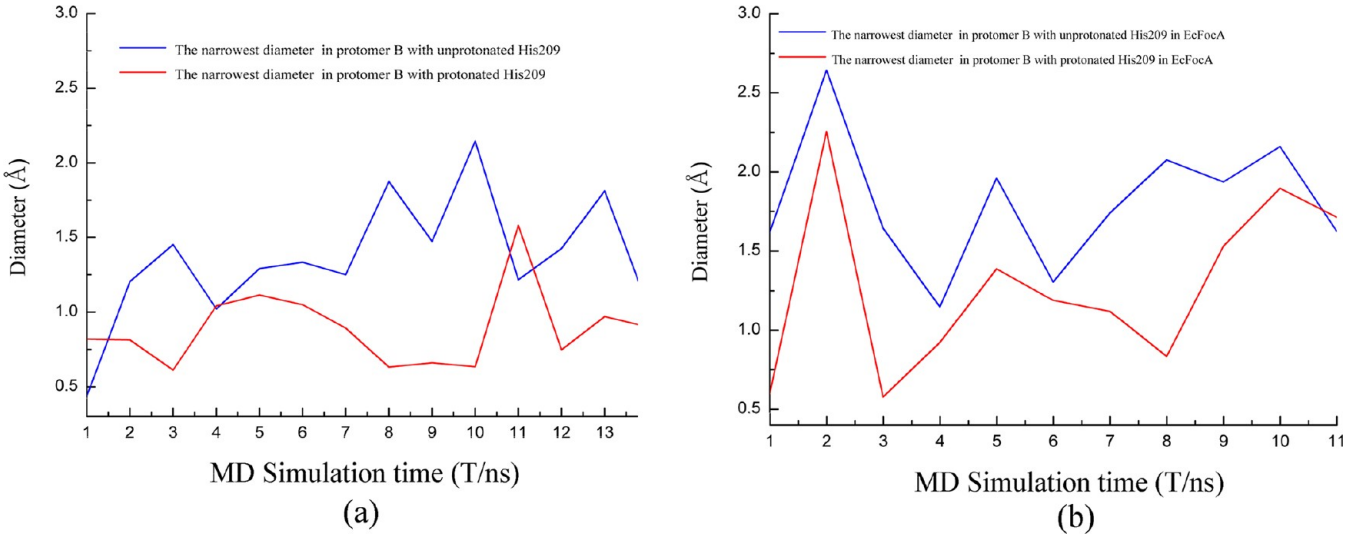

Figure 16. Diameter of the narrowest part of the formate channel in protomer B for (a) StFocA and (b) EcFocA, which was found to be smaller at low pH. The blue lines are from MD simulations at neutral/high pH (unprotonated His209), whereas the red lines are from MD simulations at low pH (protonated His209).

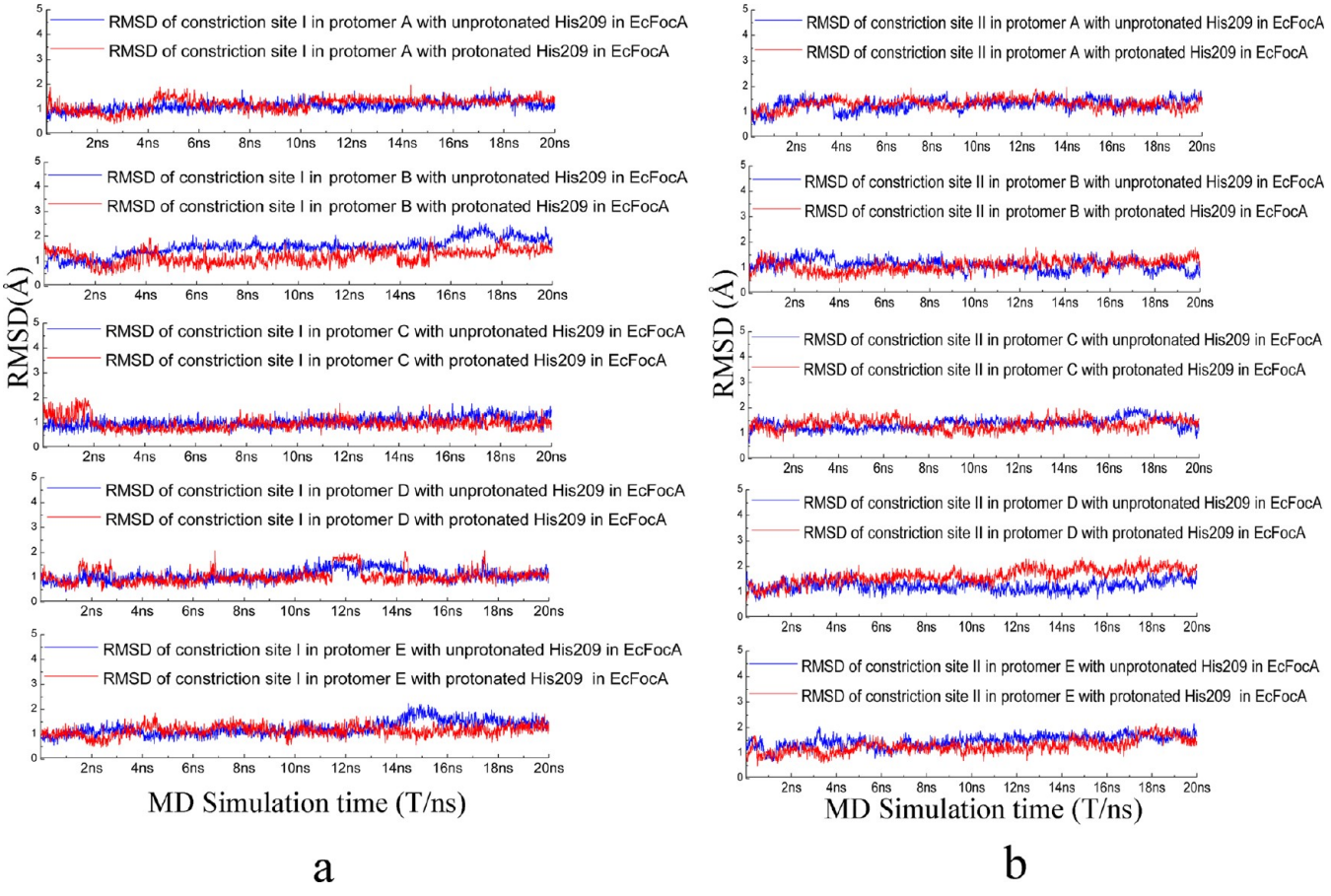

Figure 17. Time evolutions of the rmsd values of constriction sites (a) I and (b) II in each protomer of EcFocA, showing that both constriction sites become less flexible with protonated His209.

dx.doi.org/10.1021/ci300250q | J. Chem. Inf. Model. 2012, 52, 2119−2131

channel. Figure 15 shows that the rmsd values of constriction site II of protomer B are larger with protonated His209 than with unprotonated His209. Other protomers showed similar behavior (Figure S6, Supporting Information).

In summary, protonated His209 interacts tightly with its neighboring residue Asn262. The tight interaction between protonated His209 and Asn262 makes constriction site I large. However, both constriction sites I and II become more rigid. With protonated His209, the channel becomes more rigid, making formate hardly able to pass through the channel.

3.5. Simulation of EcFocA with Unprotonated or Protonated His209. As for StFocA, we performed 20-ns MD simulations of EcFocA (the sequence identity and sequence similarity between EcFocA and StFocA are 85.2% and 88.2%, respectively) with lipid and water with protonated His209 and unprotonated His209.

We also calculated the diameters of the pore in each protomer for 11 frames using HOLE[24,50] and summarize the results in Tables S3 and S4 (Supporting Information).

Although there are no N-terminal helices in EcFocA, we did not observe interactions between pairs of neighboring protomers and conformational changes. However, we also found that protomer B in EcFocA changes in a pH-dependent way as in StFocA (Figure 16). The diameter of the narrowest part of the formate channel in protomer B of EcFocA and StFocA is smaller at low pH (Figure 16), and protomer B gates in a pH-dependent way. Because of their high sequence identity and sequence similarity, these two FocA units might exhibit many similarities in gating mechanism.

For EcFocA, we also found that the diameter of the channel of constriction site I was larger at low pH than at neutral/high pH. (More details can be seen in Tables S3 and S4, Supporting Information.) Constriction sites I and II were found to become less flexible at low pH (Figure 17a,b). For His209 forming H-bonds, we obtained similar results for EcFocA as for StFocA (Figure S7, Supporting Information).

However, our MD results showed different degrees of conformational change for EcFocA and StFocA under different pH conditions, because the crystal structure of EcFocA was obtained at pH ≈ 7.5 whereas the crystal structure of StFocA was obtained at pH ≈ 4.0.

We used the vmdICE[53] program to obtain the rmsd for each residue. Here, we chose TM2a (residues Tyr64−Cys85) and the Ω loop [residues Gly86−(Leu89)−Thr91], which directly influence the axial channel in each protomer, including important residues. Figures 18 and 19 show the ColorPlot in protomer B at different pH values for StFocA and EcFocA, respectively. StFocA shows stronger conformational changes at neutral/high pH than at low pH (Figure 18 for protomer B of StFocA). In contrast, EcFocA shows stronger conformational changes at low pH than at neutral/high pH (Figure 19 for protomer B of EcFocA). Other protomers showed similar behaviors (Figures S8 and S9, Supporting Information). This can be explained by the fact that the crystal structure of StFocA

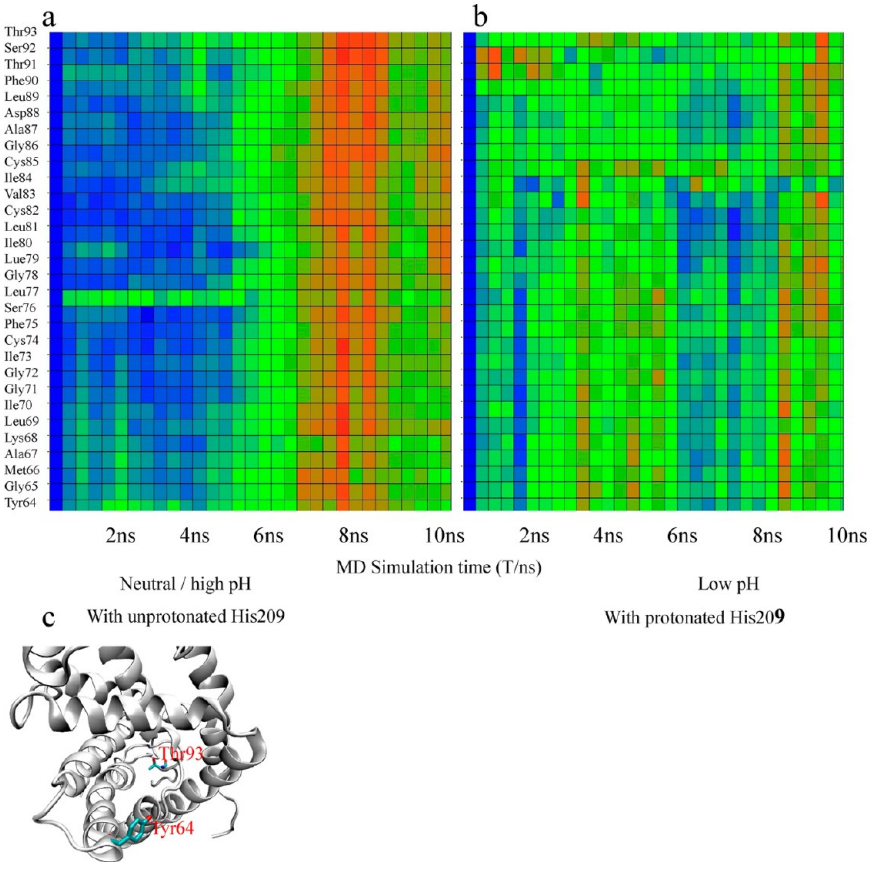

Figure 18. Comparison to the first frame of our simulation of the rmsd values of all residues (residues Tyr64−Cys91) in protomer B of StFocA, showing stronger conformational changes at (a) neutral/high pH than at (b) low pH. Time *T* (ns) is presented on the *x* axis, residues are presented on the *y* axis, and colored data points refer to different rmsd values, with red representing a high value (rmsd = 3.8 Å), green representing a medium value (rmsd = 2.3 Å), and blue representing a low value (rmsd = 1.1 Å). (c) Tyr64−Thr93 motif in protomer B of StFocA.

dx.doi.org/10.1021/ci300250q | J. Chem. Inf. Model. 2012, 52, 2119−2131

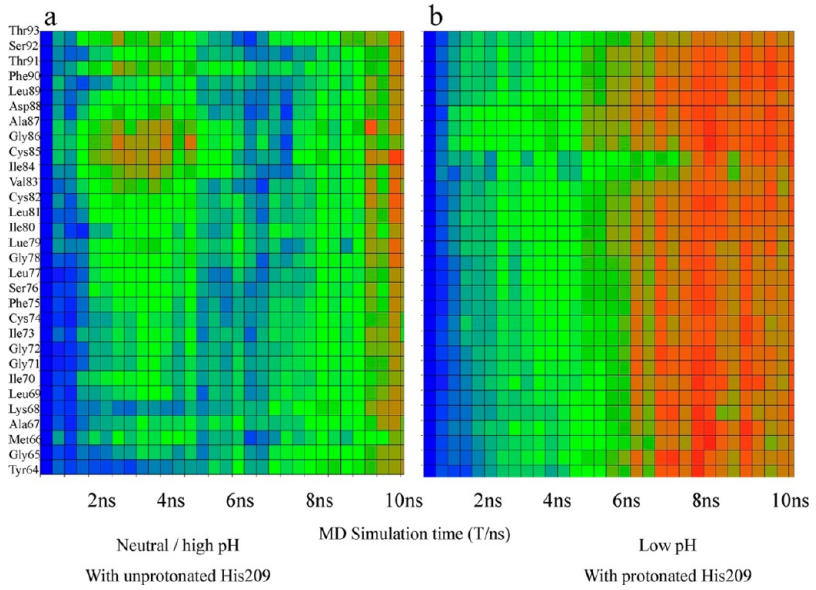

Figure 19. Comparison to the first frame of our simulation of the rmsd values of all residues (residues Tyr64−Cys91) in protomer B of EcFocA. EcFocA shows weaker conformational changes at (a) neutral/high pH than at (b) low pH. Time T (ns) is presented on the x axis, residues are presented on the y axis, and colored data points refer to different rmsd values, with red representing a high value (rmsd = 3.8 Å), green representing a medium value (rmsd = 2.3 Å), and blue representing a low value (rmsd = 1.1 Å).

was obtained at pH ≈ 4.0 whereas the crystal structure of EcFocA was obtained under pH ≈ 7.5.

4. CONCLUSIONS

Based on the recently available high resolution structures of EcFocA, VcFocA, and StFocA, we first defined the diameter of the entrance of the transport channel. Then, we performed MD simulations of the structures of EcFocA and StFocA. Our MD simulations of StFocA showed that, at neutral/high pH (MD simulation with unprotonated His209), the concerted movement of the N-terminal helices of a pair of protomers (A/B) of StFocA opens its formate channel. At low pH (MD simulation with protonated His209), protonated His209 interacts tightly with its neighboring residue Asn262, and the channel becomes narrower, making the formate hardly able to pass through the channel. We obtained similar results for EcFocA. Our study shows that pairs of protomers (A/B, C/D) in FocA move in a concerted fashion to achieve its pH-dependent gating function, which is consistent with the studies of aquaporins and provides information on the dynamics of the gating mechanism.

■ ASSOCIATED CONTENT

Supporting Information

Figures showing the central pore in crystal structure StFocA (Figure S1); equilibration of the simulation systems within 4 ns (Figure S2); five protomers under different pH conditions (Figure S3); concerted movements of protomers C and D (Figure S4); time evolutions of the rmsd values of constriction sites I (Figure S5) and II (Figure S6); hydrogen-bond distances between His209 and Asn262 in five protomers in EcFocA (Figure S7); rmsd values of each residue in StFocA (Figure S8) and EcFocA (Figure S9); important residues of the axial pore in EcFocA, VcFocA, and StFocA (Figure S10); comparison of the five protomers' loops (Figure S11). Tables listing 14 frames of data for StFocA at neutral/high pH (Table S1) and at low pH (Table S2) and 11 frames of data for EcFocA at neutral/high pH (Table S3) and at low pH (Table S4). This material is available free of charge via the Internet at http://pubs.acs.org.

■ AUTHOR INFORMATION

Corresponding Author

*E-mail: yyli@suda.edu.cn.

Notes

The authors declare no competing financial interest.

■ ACKNOWLEDGMENTS

We acknowledge support from the National Basic Research Program of China (973 Program, Grants 2012CB932400 and 2010CB934500); the National Natural Science Foundation of China (Grant 21003091); and the Natural Science Foundation of Jiangsu Province (Grant BK2010216), a Project Funded by the Priority Academic Program Development of Jiangsu Higher Education Institutions (PAPD).

■ REFERENCES

(1) King, L. S.; Kozono, D.; Agre, P. From structure to disease: The evolving tale of aquaporin biology. *Nat. Rev. Mol. Cell Biol.* **2004**, *5*, 687−698.

(2) Maurel, C.; Verdoucq, L.; Luu, D. T.; Santoni, V. Plant aquaporins: Membrane channels with multiple integrated functions. *Annu. Rev. Plant Biol.* **2008**, *59*, 595−624.

(3) Agre, P.; King, L. S.; Yasui, M.; Guggino, W. B.; Ottersen, O. P.; Fujiyoshi, Y.; Engel, A.; Nielsen, S. Aquaporin water channels—From atomic structure to clinical medicine. *J. Physiol.* **2002**, *542*, 3−16.

(4) Litman, T.; Sogaard, R.; Zeuthen, T. Ammonia and urea permeability of mammalian aquaporins. *Handb. Exp. Pharmacol.* **2009**, *190*, 327−358.

(5) Yasui, M. pH regulated anion permeability of aquaporin-6. *Handb. Exp. Pharmacol.* **2009**, *190*, 299−308.

(6) Zardoya, R. Phylogeny and evolution of the major intrinsic protein family. *Biol. Cell* **2005**, *97*, 397−414.

(7) Ishibashi, K. New members of mammalian aquaporins: AQP10-AQP12. *Handb. Exp. Pharmacol.* **2009**, *190*, 251−262.

(8) Carbrey, J. M.; Agre, P. Discovery of the aquaporins and development of the field. *Handb. Exp. Pharmacol.* **2009**, *190*, 3−28.
(9) Cerda, J.; Finn, R. N. Piscine aquaporins: An overview of recent advances. *J. Exp. Zool. A: Ecol. Genet. Physiol.* **2010**, *313*, 623−650.
(10) Fu, D.; Libson, A.; Miercke, L. J.; Weitzman, C.; Nollert, P.; Krucinski, J.; Stroud, R. M. Structure of a glycerol-conducting channel and the basis for its selectivity. *Science* **2000**, *290*, 481−486.
(11) Sui, H.; Han, B. G.; Lee, J. K.; Walian, P.; Jap, B. K. Structural basis of water-specific transport through the AQP1 water channel. *Nature* **2001**, *414*, 872−878.
(12) Harries, W. E.; Akhavan, D.; Miercke, L. J.; Khademi, S.; Stroud, R. M. The channel architecture of aquaporin 0 at a 2.2-Å resolution. *Proc. Natl. Acad. Sci. U.S.A.* **2004**, *101*, 14045−14050.
(13) Leonhartsberger, S.; Korsa, I.; Bock, A. The molecular biology of formate metabolism in enterobacteria. *J. Mol. Microbiol. Biotechnol.* **2002**, *4*, 269−276.
(14) Sawers, R. G. Formate and its role in hydrogen production in *Escherichia coli*. *Biochem. Soc. Trans.* **2005**, *33*, 42−46.
(15) Stams, A. J.; Plugge, C. M. Electron transfer in syntrophic communities of anaerobic bacteria and archaea. *Nat. Rev. Microbiol.* **2009**, *7*, 568−577.
(16) Saier, M. H., Jr.; Eng, B. H.; Fard, S.; Garg, J.; Haggerty, D. A.; Hutchinson, W. J.; Jack, D. L.; Lai, E. C.; Liu, H. J.; Nusinew, D. P.; Omar, A. M.; Pao, S. S.; Paulsen, I. T.; Quan, J. A.; Sliwinski, M.; Tseng, T. T.; Wachi, S.; Young, G. B. Phylogenetic characterization of novel transport protein families revealed by genome analyses. *Biochim. Biophys. Acta* **1999**, *1422*, 1−56.
(17) Clegg, S.; Yu, F.; Griffiths, L.; Cole, J. A. The roles of the polytopic membrane proteins NarK, NarU and NirC in *Escherichia coli* K-12: Two nitrate and three nitrite transporters. *Mol. Microbiol.* **2002**, *44*, 143−155.
(18) Clegg, S. J.; Jia, W.; Cole, J. A. Role of the *Escherichia coli* nitrate transport protein, NarU, in survival during severe nutrient starvation and slow growth. *Microbiology* **2006**, *152*, 2091−2100.
(19) Jia, W.; Cole, J. A. Nitrate and nitrite transport in *Escherichia coli*. *Biochem. Soc. Trans.* **2005**, *33*, 159−161.
(20) Jia, W.; Tovell, N.; Clegg, S.; Trimmer, M.; Cole, J. A single channel for nitrate uptake, nitrite export and nitrite uptake by *Escherichia coli* NarU and a role for NirC in nitrite export and uptake. *Biochem. J.* **2009**, *417*, 297−304.
(21) Gates, A. J.; Luque-Almagro, V. M.; Goddard, A. D.; Ferguson, S. J.; Roldan, M. D.; Richardson, D. J. A composite biochemical system for bacterial nitrate and nitrite assimilation as exemplified by Paracoccus denitrificans. *Biochem. J.* **2011**, *435*, 743−753.
(22) Beckham, K. S.; Potter, J. A.; Unkles, S. E. Formate-nitrite transporters: Optimization of expression, purification and analysis of prokaryotic and eukaryotic representatives. *Protein Expression Purif.* **2010**, *71*, 184−189.
(23) Nolling, J.; Reeve, J. N. Growth- and substrate-dependent transcription of the formate dehydrogenase (fdhCAB) operon in *Methanobacterium thermoformicicum* Z-245. *J. Bacteriol.* **1997**, *179*, 899−908.
(24) Smart, O. S.; Neduvelil, J. G.; Wang, X.; Wallace, B. A.; Sansom, M. S. HOLE: A program for the analysis of the pore dimensions of ion channel structural models. *J. Mol. Graph.* **1996**, *14*, 354−360.
(25) Law, C. J.; Maloney, P. C.; Wang, D. N. Ins and outs of major facilitator superfamily antiporters. *Annu. Rev. Microbiol.* **2008**, *62*, 289−305.
(26) Sawers, R. Formate and its role in hydrogen production in *Escherichia coli*. *Biochem. Soc.T.* **2005**, *33*, 42−46.
(27) Suppmann, B.; Sawers, G. Isolation and characterization of hypophosphite-resistant mutants of *Escherichia coli*: Identification of the FocA protein, encoded by the pfl operon, as a putative formate transporter. *Mol. Microbiol.* **1994**, *11*, 965−982.
(28) Wang, Y.; Huang, Y.; Wang, J.; Cheng, C.; Huang, W.; Lu, P.; Xu, Y. N.; Wang, P.; Yan, N.; Shi, Y. Structure of the formate transporter FocA reveals a pentameric aquaporin-like channel. *Nature* **2009**, *462*, 467−472.
(29) Waight, A. B.; Love, J.; Wang, D. N. Structure and mechanism of a pentameric formate channel. *Nat. Struct. Mol. Biol.* **2009**, *17*, 31−37.
(30) Lu, W.; Du, J.; Wacker, T.; Gerbig-Smentek, E.; Andrade, S. L.; Einsle, O. pH-dependent gating in a FocA formate channel. *Science* **2011**, *332*, 352−354.
(31) Mathai, J. C.; Tristram-Nagle, S.; Nagle, J. F.; Zeidel, M. L. Structural determinants of water permeability through the lipid membrane. *J. Gen. Physiol.* **2008**, *131*, 69−76.
(32) Murata, K.; Mitsuoka, K.; Hirai, T.; Walz, T.; Agre, P.; Heymann, J. B.; Engel, A.; Fujiyoshi, Y. Structural determinants of water permeation through aquaporin-1. *Nature* **2000**, *407*, 599−605.
(33) Garate, J. A.; English, N. J.; MacElroy, J. M. Human aquaporin 4 gating dynamics in dc and ac electric fields: A molecular dynamics study. *J. Chem. Phys.* **2011**, *134*, 055110.
(34) Han, B. G.; Guliaev, A. B.; Walian, P. J.; Jap, B. K. Water transport in AQP0 aquaporin: Molecular dynamics studies. *J. Mol. Biol.* **2006**, *360*, 285−296.
(35) Hub, J. S.; Grubmuller, H.; de Groot, B. L. Dynamics and energetics of permeation through aquaporins. What do we learn from molecular dynamics simulations? *Handb. Exp. Pharmacol.* **2009**, *190*, 57−76.
(36) Xin, L.; Su, H.; Nielsen, C. H.; Tang, C.; Torres, J.; Mu, Y. Water permeation dynamics of AqpZ: A tale of two states. *Biochim. Biophys. Acta* **2011**, *1808*, 1581−1586.
(37) Zhu, F.; Tajkhorshid, E.; Schulten, K. Pressure-induced water transport in membrane channels studied by molecular dynamics. *Biophys. J.* **2002**, *83*, 154−160.
(38) *Studio D*, version 2.5; Accelrys Inc.: San Diego, CA, 2007.
(39) Jorgensen, W. L.; Chandrasekhar, J.; Madura, J. D.; Impey, R. W.; Klein, M. L. Comparison of simple potential functions for simulating liquid water. *J. Chem. Phys.* **1983**, *79*, 926.
(40) Hsin, J.; Arkhipov, A.; Yin, Y.; Stone, J. E.; Schulten, K. Using VMD: An introductory tutorial. In *Current Protocols in Bioinformatics*; Wiley: New York, 2008; Chapter 5.
(41) Kalé, L.; Skeel, R.; Bhandarkar, M.; Brunner, R.; Gursoy, A.; Krawetz, N.; Phillips, J.; Shinozaki, A.; Varadarajan, K.; Schulten, K. NAMD2: Greater Scalability for Parallel Molecular Dynamics. *J. Comput. Phys.* **1999**, *151*, 283−312.
(42) MacKerell, A. D.; Bashford, D.; Bellott, M.; Dunbrack, R. L.; Evanseck, J. D.; Field, M. J.; Fischer, S.; Gao, J.; Guo, H.; Ha, S.; Joseph-McCarthy, D.; Kuchnir, L.; Kuczera, K.; Lau, F. T. K.; Mattos, C.; Michnick, S.; Ngo, T.; Nguyen, D. T.; Prodhom, B.; Reiher, W. E.; Roux, B.; Schlenkrich, M.; Smith, J. C.; Stote, R.; Straub, J.; Watanabe, M.; Wiorkiewicz-Kuczera, J.; Yin, D.; Karplus, M. All-atom empirical potential for molecular modeling and dynamics studies of proteins. *J. Phys. Chem. B* **1998**, *102*, 3586−3616.
(43) Brooks, B. R.; Bruccoleri, R. E.; Olafson, B. D. CHARMM: A program for macromolecular energy, minimization, and dynamics calculations. *J. Comput. Chem.* **1983**, *4*, 187−217.
(44) Feller, S. E.; MacKerell, A. D. An improved empirical potential energy function for molecular simulations of phospholipids. *J. Phys. Chem. B* **2000**, *104*, 7510−7515.
(45) Essmann, U.; Perera, L.; Berkowitz, M. L.; Darden, T.; Lee, H.; Pedersen, L. G. A smooth particle mesh Ewald method. *J. Chem. Phys.* **1995**, *103*, 8577−8593.
(46) Feng, Z.; Hou, T.; Li, Y. Studies on the Interactions between β2 Adrenergic Receptor and Gs Protein by Molecular Dynamics Simulations. *J. Chem. Inf. Model.* **2012**, *52*, 1005−1014.
(47) Li, Y.; Hou, T.; Goddard, I. Computational modeling of structure−function of G protein-coupled receptors with applications for drug design. *Curr. Med. Chem.* **2010**, *17*, 1167−1180.
(48) Li, Y.; Hou, T. Computational Simulation of Drug Delivery at Molecular Level. *Curr. Med. Chem.* **2010**, *17*, 4482−4491.
(49) Li, Y.; Zhu, F.; Vaidehi, N.; Goddard, W. A., III; Sheinerman, F.; Reiling, S.; Morize, I.; Mu, L.; Harris, K.; Ardati, A. Prediction of the 3D structure and dynamics of human DP G-protein coupled receptor bound to an agonist and an antagonist. *J. Am. Chem. Soc.* **2007**, *129*, 10720−10731.

(50) Smart, O. S.; Goodfellow, J. M.; Wallace, B. A. The pore dimensions of gramicidin A. *Biophys. J.* **1993**, *65*, 2455−2460.
(51) Tipmanee, V.; Blumberger, J. Kinetics of the Terminal Electron Transfer Step in Cytochrome C Oxidase. *J. Phys. Chem. B* **2012**, *116*, 1876−1883.
(52) Dubey, K. D.; Chaubey, A. K.; Ojha, R. P. Role of pH on dimeric interactions for DENV envelope protein: An insight from molecular dynamics study. *Biochim. Biophys. Acta* **2011**, *1814*, 1796−1801.
(53) Knapp, B.; Lederer, N.; Omasits, U.; Schreiner, W. vmdICE: A Plug-In for Rapid Evaluation of Molecular Dynamics Simulations using VMD. *J. Comput. Chem.* **2010**, *31*, 2868−2873.